ACS SENSORS

pubs.acs.org/acssensors

Article

A Supported Lipid Bilayer-Based Lab-on-a-Chip Biosensor for the Rapid Electrical Screening of Coronavirus Drugs

Feng Zhou, Wenwei Pan, Ye Chang, Xueyou Su, Xuexin Duan,* and Qiannan Xue*

Cite This: https://doi.org/10.1021/acssensors.2c00970

Read Online

ACCESS | Metrics & More | Article Recommendations | Supporting Information

ABSTRACT: With the rapid spread and multigeneration variation of coronavirus, rapid drug development has become imperative. A major obstacle to addressing this issue is adequately constructing the cell membrane at the molecular level, which enables in vitro observation of the cell response to virus and drug molecules quantitatively, shortening the drug experiment cycle. Herein, we propose a rapid and label-free supported lipid bilayer-based lab-on-a-chip biosensor for the screening of effective inhibition drugs. An extended gate electrode was prepared and functionalized by an angiotensin-converting enzyme II (ACE2) receptor-incorporated supported lipid bilayer (SLB). Such an integrated system can convert the interactions of targets and membrane receptors into real-time charge signals. The platform can simulate the cell membrane microenvironment in vitro and accurately capture the interaction signal between the target and the cell membrane with minimized interference, thus observing the drug action pathway quantitatively and realizing drug screening effectively. Due to these label-free, low-cost, convenient, and integrated advantages, it is a suitable candidate method for the rapid drug screening for the early treatment and prevention of worldwide spread of coronavirus.

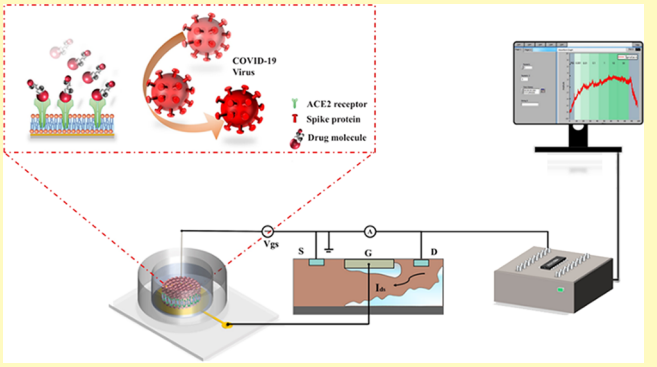

KEYWORDS: *lipid bilayers, lab-on-a-chip, drugs screening, coronavirus drugs, extended gate-type FET*

As the number of cases continues to increase, the novel coronavirus mutates rapidly and the vaccine development cannot catch up with the rate of the virus mutation; hence, the rapid development of therapeutic drugs is urgently needed. Recent reports have revealed that SARS-CoV-2 infects host cells by binding to the angiotensin-converting enzyme II (ACE2) receptor on the surface of human and animal cells[1−3] and exhibits ∼10- to 20-fold higher affinity than that of the ACE2 receptor binding to SARS-CoV.[4] The effects of drugs and viruses on cells can be reflected by cell culture fluorescence quantification.[5] Researchers can only draw fuzzy conclusions from statistical experiments, which cannot accurately analyze the interaction between viruses and human cells. Methods such as surface plasmon resonance[6,7] and interferometry[8] are also good candidates, which are label-free and shorten the detection cycle. However, they are either expensive or the system is complex and difficult to promote in bulk. Therefore, a simple and rapid platform used for simulating the interaction of viral pathogens and the screening of effective inhibition drugs will be of great significance for the treatment and prevention of various widespread epidemics.

For environmental monitoring and medical diagnostics, field effect transistors (FETs) were introduced owing to their sensitivity, low cost, fast response, and scaled integrability, which have been widely used in label-free protein detection, enzyme reactions, ion channels, pH detection, etc.[9−12] The separation of the gate electrode and the metal oxide−semiconductor field-effect transistor (MOSFET) of an extended gate-type field-effect transistor not only improves the stability of the MOSFET electrical unit, avoiding environmental interference, such as light, temperature, and chemical erosion, but also facilitates the physical structures,[13−15] chemical materials,[16−18] and biological molecules[19,20] coated on the gate electrode. However, the Debye screening length modulation and nonspecific binding of the unforeseen analyte may still result in unstable detection and quantitation of targets.

The employment of supported lipid bilayers (SLBs) is a typical method for investigating viral infection, signal transduction, and drug delivery at the molecular level. Distinguishing from sophisticated cell models, an SLB provides a robust and simplified alternative for studying cell membrane behaviors. By incorporating membrane receptors, the SLB can provide new insights into the investigation of membrane

Received: May 4, 2022
Accepted: June 15, 2022

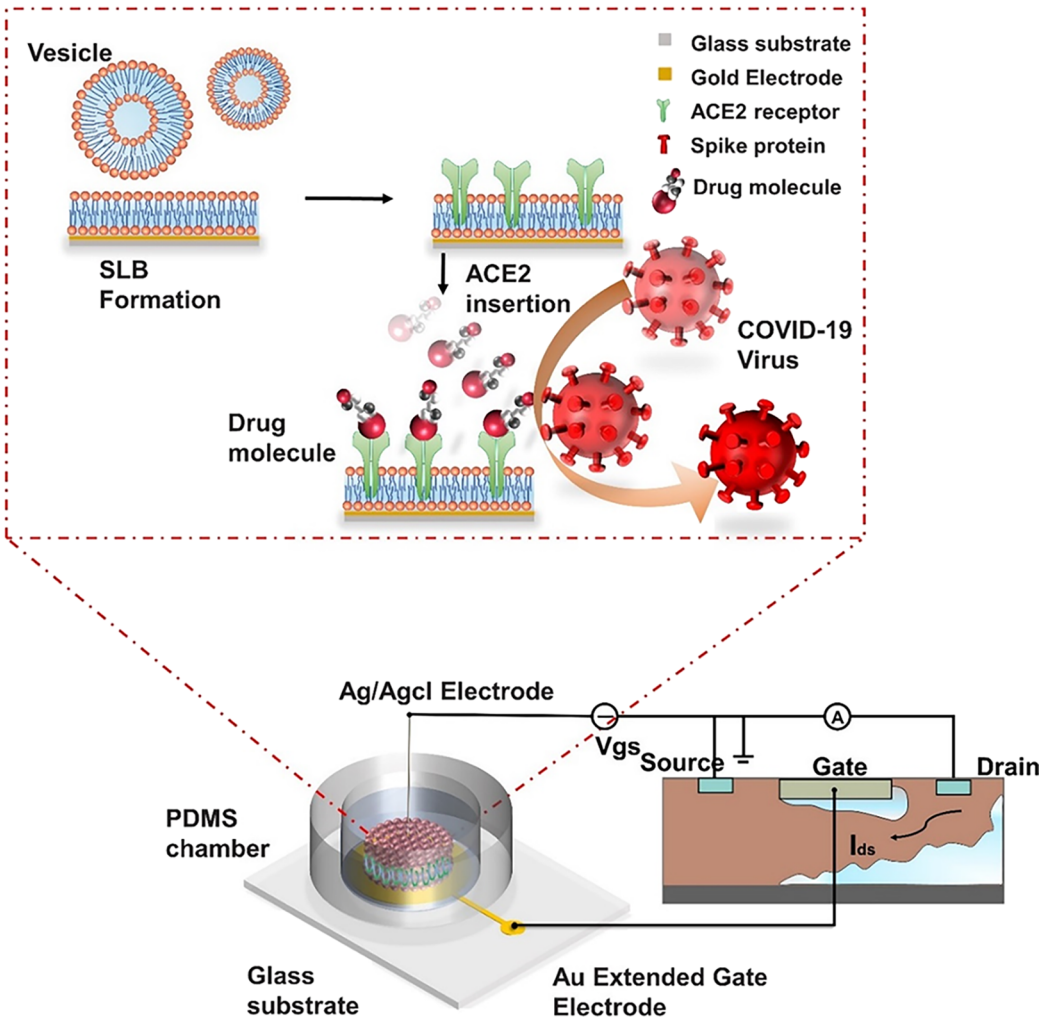

Figure 1. Schematic illustration of the binding process and the detection electrical circuit scheme: SLB formation, ACE2 receptor insertion, and competition between drug molecules and spike proteins or viruses.

behavior, including ion transport,[21−23] virus detection,[24−27] substrate−enzyme reactions,[28,29] antigen−antibody bonds,[30,31] and protein−protein interactions.[32,33]

In this study, we propose a rapid and label-free SLB-based lab-on-a-chip biosensor for the analysis of virus−cell membrane interactions and screening for effective inhibition drugs. Compared with using the receptors immobilized directly on the solid substrate to quantify the blocking effect of drugs on virus binding, SLB modification can provide a biomimetic and cell-simulating environment, isolating the interference and avoiding nonspecific binding. We demonstrated an extended-gate field-effect transistor (EGFET)-based biosensor functionalized with a receptor-incorporated SLB, which enables rapid, low-cost, label-free detection and drug screening. The SLB was employed as a biomimetic cell membrane owing to its intrinsic properties, such as morphological stability, electrical conductivity, lateral fluidity, and analyte permeability. ACE2 receptors were incorporated into the SLB membrane to functionalize the sensing interface and simulate human cells locally, which combines FET to effectively shield noise within the Debye length distance and realize stable charge signal capture due to the uniformity of the lipid film and constant height and orientation of ACE2. Owing to the rapid and sensitive response, the proposed biosensor can monitor the binding of the spike protein to the embedded receptors in real time. Most importantly, the biosensor can successfully determine the different inhibitory effects of drug molecules on the binding process, suggesting great potential and versatile capability for the early treatment and prevention of widespread epidemics.

BIOSENSOR DESIGN

Device Fabrication and Formation of the Lipid Bilayer. The extended gate unit consisted of a gold electrode layer and a chamber reservoir containing an SLB. The gold electrode layer was fabricated by graphically evaporating a circle of 8 mm in diameter and 200 nm in thickness on a glass substrate, which was used as a physically separated FET extended gate electrode, providing a flat and hydrophilic interface for the subsequent SLB formation. The chamber reservoir was made of a 10 mm annular PDMS chamber bonded to the gold electrode layer, providing shape constraints on the SLB membranes and liquid environment.

Subsequently, the SLB was paved on the plasma-processed surface of the gold layer via the vesicle fusion method (see the Supporting Information for details) and then rinsed extensively with 10 mM PBS buffer to remove the excess vesicles, which serve as a biomimetic cell membrane interface with active receptors.

https://doi.org/10.1021/acssensors.2c00970
ACS Sens. XXXX, XXX, XXX−XXX

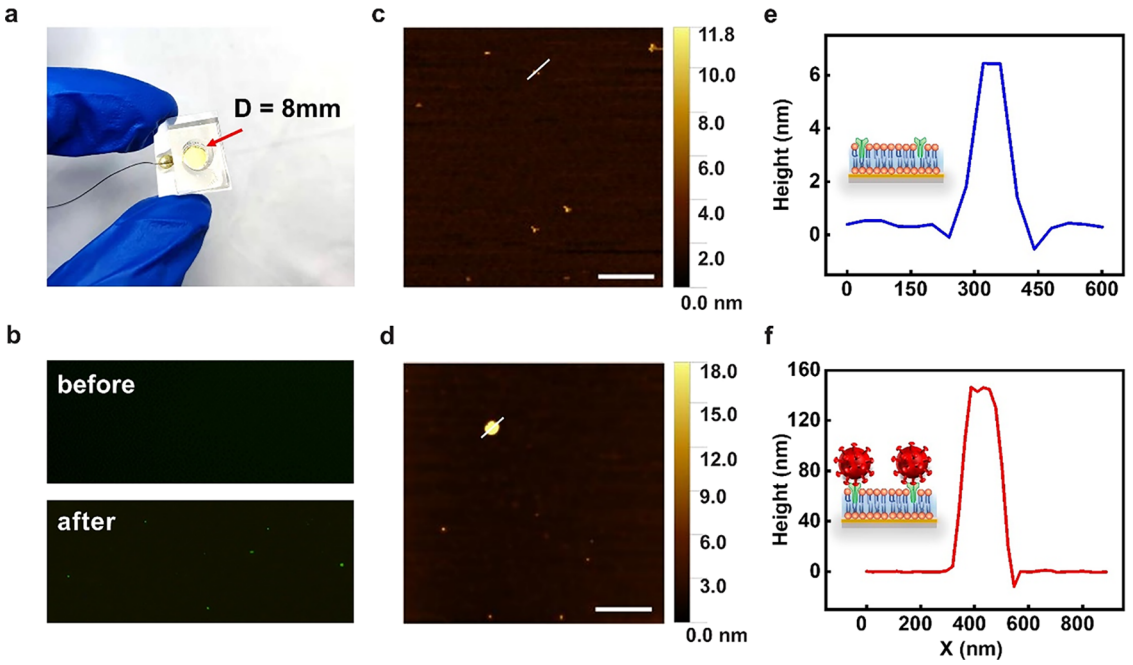

Figure 2. Characterizations of the incorporation process. (a) Photography of the fabricated device. (b) Comparison before and after the insertion of ACE2 receptors with FITC. The full images are shown in Figure S4. (c) Morphology of ACE2 receptors on a supported lipid bilayer. (d) The AFM image shows the morphology of the ACE2 receptors and coronavirus complex. Scale bars in the images denote 1 μm. (e, f) Cross sections of the ACE2 receptors (6 nm, blue line graph) and coronavirus complex (150 nm, red line graph).

Setup of the EGFET System. A gold electrode-coated button with an SLB served as an extended gate for the commercial FET (ALD1108A, USA). A tiny Ag/AgCl electrode made by electroplating was immersed into the chamber reservoir as a reference electrode to bias the transistor to the desired linear amplification voltage (0.5 V). The gate electrode was connected to a PCB circuit to enable the current trace recording.

RESULTS AND DISCUSSION

Sensing Mechanism. As shown in Figure 1, an SLB-based lab-on-a-chip biosensor comprises an extended gate unit and a field effect transistor (FET) electrical circuit unit. The gold electrode bottom retains real-time monitoring and quantification through the electrical connection between the solution and the Ag/AgCl electrode, which senses the voltage changes caused by the binding of the analyte and receptors embedded within the Debye length. Voltage changes can be obtained via eq 1:

$$\varphi = \frac{\Delta\sigma}{C_{DL} + C_{FET}} \tag{1}$$

Here, $\Delta\sigma$ is the change in stable quantity charge caused by the target captured by receptors embedded in the SLB, and φ represents the variable of gate voltage. C_{DL} and C_{FET} represent the diffuse layer capacitance and the inherent capacitance of the FET,[34] respectively (Figure S1). As shown in Figure S1, changes in the captured charge at the sensing interface are shared by the two partial capacitors, resulting in changes in gate voltage. The back-end of the bottom electrode layer was connected to the gate of the commercial FET circuit unit, and the changes in front voltage were amplified and recorded through the FET in the linear region of the transfer characteristic curve. The transfer characteristic curve is given by eq 2:

$$I_{ds} = k(V_{gs} - V_{th})V_{ds} \tag{2}$$

Here, k is the characteristic constant of the FET, V_{gs} is the gate-to-source voltage, V_{th} is the turn-on threshold voltage, and V_{ds} is the drain-to-source voltage.

The embedded image in Figure 1 shows the interface behavior during the drug screening. The bionic cell membrane simulates the process of human cell infection with coronavirus and can be combined with the spike protein of coronavirus or blocking drugs. Because the charges of the coronavirus and the blocking drug are significantly different, the change in charge on the surface of the gate electrode can be converted into an electrically detectable signal. Therefore, the electrical response can help us compare the blocking effects of different drugs, enabling the screening of drugs with a strong blocking effect of the coronavirus infection.

Debye screening length (λ_D)[35] is an existing challenge for field-effect sensor applications, as shown in eq 3:

$$\varphi = \frac{q}{r}\exp\left(-\frac{r}{\lambda_D}\right) \tag{3}$$

Here, r is the distance from the SLB to the center of the captured molecule. φ is the potential at a distance r from the source charge, implying the characteristic length of the Coulomb potential attenuation. Therefore, the stable thickness of the lipid bilayers (6 nm) and the orientation of the embedded ACE2 receptors (as shown in Figure 1) present a constant distance between the analyte binding and the detection interface, thus avoiding the fluctuation of the distance r from the charge to the electrode surface, which makes a stable electrical detection possible (eq 3).[36,37] In addition, lipid bilayers can block most of the specific binding, which is reflected in two aspects. (i) The effect of nonspecific binding on the interface charge can be avoided by flushing the buffer after the actual test to maintain the proper functioning

https://doi.org/10.1021/acssensors.2c00970
ACS Sens. XXXX, XXX, XXX−XXX

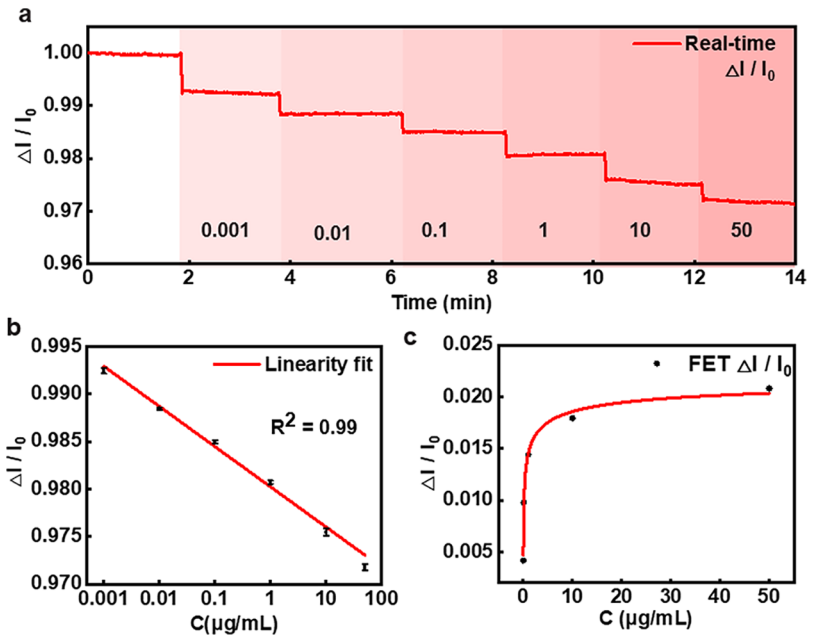

Figure 3. Real-time response of spike proteins and K_D calculation. (a) Normalized real-time FET response to the gradient spike protein. (b) Linearity fit of the FET biosensor. (c) Average FET current response of the gradient spike protein and Hill fit. Statistical test data were repeated at least three times.

of the inserted protein. (ii) Lipid bilayers protected the extended gate electrode as a sensing interface against solution erosion.[38]

In this way, different drug molecules or spike proteins have different charges, and the binding directly leads to electrical signal changes. Compared with existing instruments, the proposed biosensor has the advantages of fast response and direct sensing without indirect signal conversion.

Characterization of the Biosensing Interface. The device consists of a glass substrate, a gold electrode layer, and a PDMS chamber layer as shown in Figure 2a, which provides a sensing interface for subsequent FET electrical detection and a shape constraint for the next SLB formation. The supported lipid bilayer is fabricated by the vesicle fusion method. The vesicles automatically adsorb on the plasma-pretreated hydrophilic gold surface and shatter to form a complete SLB. The increase in electrode surface coverage leads to a gradual decline of the real-time current of FET as shown in Figure S3a. As shown in Figure S2, the process of SLB formation was monitored using commercial quartz crystal microbalance with dissipation monitoring (QCM-D) as auxiliary validation, showing a typical frequency shift of 22 Hz and a dissipation decrease of less than 0.1×10^{-6} induced by the formation of SLBs from lipid vesicles. In addition, cyclic voltammetry (Figure S3b) and fluorescence recovery after photobleaching (FRAP) (Figure S3c) were performed to characterize the integrity and bioactivity of the lipid bilayer. A significant current drop of CV curves indicates that an intact SLB was successfully modified onto the device surface. FRAP images show that the fluorescence-labeled SLB moves laterally to the bleached area immediately after intense laser irradiation, indicating the good quality and bioactivity of the SLB. Next, the concentration and assembly time of ACE2 receptors were optimized, as shown in Figure S5, indicating that the optimal embedding was achieved at 1 μg/mL for 30 min. Then, the ACE2 receptor solution (1 μg/mL) was added to the SLB membrane and incubated for 30 min to obtain lipid bilayers with homogeneous ACE2 receptor distribution.

To evaluate the effect of assembly, fluorescence microscopy and AFM were employed to demonstrate the horizontal distribution of ACE2 receptors and depict the vertical height profile, respectively. As shown in Figure 2b, after an SLB was fully incubated with ACE2 receptors labeled with FITC and extensive PBS washing, it showed an obvious uniform green fluorescence bright spot compared with the only SLB, indicating the successful assembly of ACE2 receptors and uniform lateral distribution. AFM was also used to delineate the distribution and height of ACE2 morphologically. SLBs were incubated with ACE2 at a concentration of 0.01 μg/mL after washing thoroughly. The height of the ACE2 receptors on the SLB was approximately 6 nm as shown in the cross section of Figure 2e.

Subsequently, we also conducted the control group after the ACE2 receptors of the sensing interface bonded with transmissible gastroenteritis virus (TGEV). TGEV belongs to the genus Alphacoronavirus 1 with a diameter of 150 nm and a coronavirus structure similar to that of SARS-CoV-2, which contains the spike (S), envelope (E), membrane (M), and nucleocapsid (N) proteins. After the insertion of ACE2 receptors, 1 μg/mL coronavirus solution was added and incubated for 30 min. After the replacement of the solution again, the AFM morphology and cross line section of coronavirus are shown in Figure 2d,f, which show values that are very close to the previously reported values of height and size (150 nm). In addition, the adsorption density of ACE2 protein measured by AFM was consistent with the frequency shift signal of QCM-D, indicating the successful modification of ACE2.

All these results demonstrate that ACE2 receptors were successfully embedded in the SLB-based biosensor, which also showed the capability to capture spike proteins.

Sensitive Capture of Spike Proteins. To characterize the ability of the biosensor to monitor and quantitate the

https://doi.org/10.1021/acssensors.2c00970
ACS Sens. XXXX, XXX, XXX−XXX

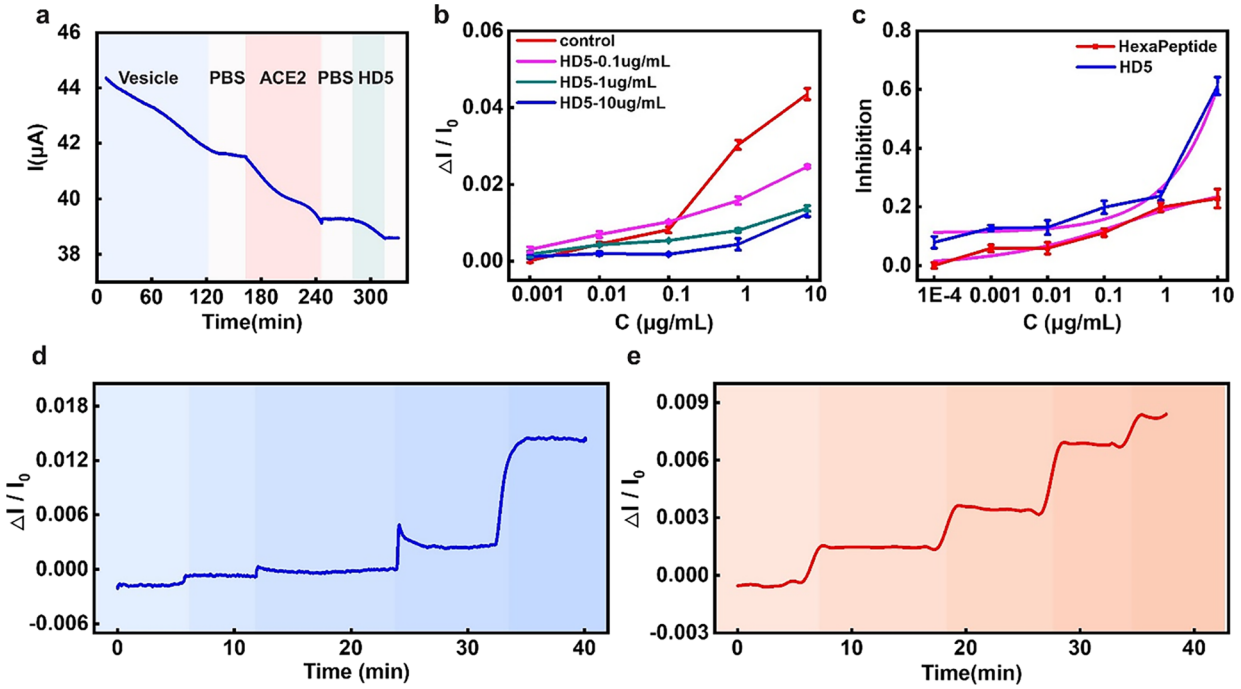

Figure 4. Feasibility verification for the drug screening of the SLB-based lab-on-a-chip biosensor. (a) Real-time FET results of the SLB formation, ACE2 receptor insertion, and HD5 peptide binding. (b) FET results of the drug inhibition efficiency of spike protein interaction with ACE2 receptors at three different concentrations. (c) FET current response of inhibition of the two drugs and their four-parameter formula model IC_{50} fit. (d, e) Real-time FET response of HD5 (d) and hexapeptide (e) interaction with the chip. Statistical test data were repeated at least three times.

interaction between the modified receptors and target analytes, we performed the binding experiment of ACE2 receptors and spike proteins on the SLB-based biosensor to preliminarily demonstrate the sensitive ability to capture. SLB and ACE2 receptors were assembled on the gold sensitive layer as mentioned above, and then the gradient spike proteins ranging from 0.001 to 50 μg/mL (0.001, 0.01, 0.1, 1, 12, 25, and 50 μg/mL, corresponding to 0.013, 0.13, 1.26, 12.56, 75.38, 314.07, and 628.14 nM in molar concentration, respectively) were added to the chip surface, respectively. Figure 3a shows the real-time FET response of the gradient spike protein. The current continues to decrease with the increase in spike protein concentration due to the negatively charged spike protein (−23.8 mV). In the specific control experiment, the introduction of nontarget molecules on the sensor surface causes a rather smaller response compared with the target with a spike protein, indicating the brilliant specificity of the sensor interface (Figure S6). The relationship between the sensor normalized response $\Delta I/I_0$ and the concentration shows excellent sensitivity (84.4 nA/ log c[s protein]) and linearity (R^2 = 0.99), as shown in Figure 3b.

To characterize the sensitive quantitative ability to target analytes, we conducted the calculation experiment of binding affinity. The relationship between the statistical average responses under gradient spike protein concentrations is shown in Figure 3c. Due to the fact that $\Delta I/I_0 \propto n$, we employed the Langmuir equation (eq 4) to fit all the experimental results, as follows:

$$\theta = \frac{C}{(K_D + C)} \tag{4}$$

Here, θ is the response of the different detection methods. C is the concentration of the introduced spike protein. The fitting process was based on the following assumptions: (1) Fixed receptors are uniformly distributed in the SLB. Each binding site has the same binding capacity and can only capture one spike protein molecule or virus with a spike protein, which means that the Hill coefficient is 1. (2) ACE2 receptors, spike proteins, and coronavirus are rigid in buffer solutions; as shown in Figure 3c, the average response fits well with the spike concentrations when using the Langmuir equation (R^2 = 0.998).

Through statistical averaging, the K_D value was calculated to be approximately 1.531 nM through the current response $\Delta I/I_0$ of our FET biosensor, which is similar to the biolayer interferometry (BLI) results reported.[37] To verify the performance of the proposed biosensor, the same SLB formation, ACE2 assembly, and spike protein capture were also conducted on the gold sensitive surface of QCM-D and surface plasmon resonance (SPR), respectively. The real-time response and the fitting of statistical results are shown in Figure S7. Through statistical averaging as shown in Figure 3d, the K_D value was calculated to be approximately 24.871 nM of SPR and 6.288 nM of QCM-D, which are close to the FET results. Compared with the lower detection limit of QCM (62.5 pM), the lower detection limit of our proposed FET method is 2.5 pM. The higher sensitivity and lower detection limit of the proposed FET method may be attributed to its sensing mechanism based on the detection of transient charge changes during interaction with target analytes. The electrical sensing mechanism exhibits two obvious advantages. One is that the direct Coulomb interactions make detection more rapid; the other is that the threshold of the minimum analyte that can be sensing is smaller due to the high precision of electricity, which endows the FET sensor with faster and more sensitive detection ability. In addition, the SLB-based FET biosensor can not only shield the interference of nonspecific binding but also can be used to monitor the translocation

https://doi.org/10.1021/acssensors.2c00970
ACS Sens. XXXX, XXX, XXX−XXX

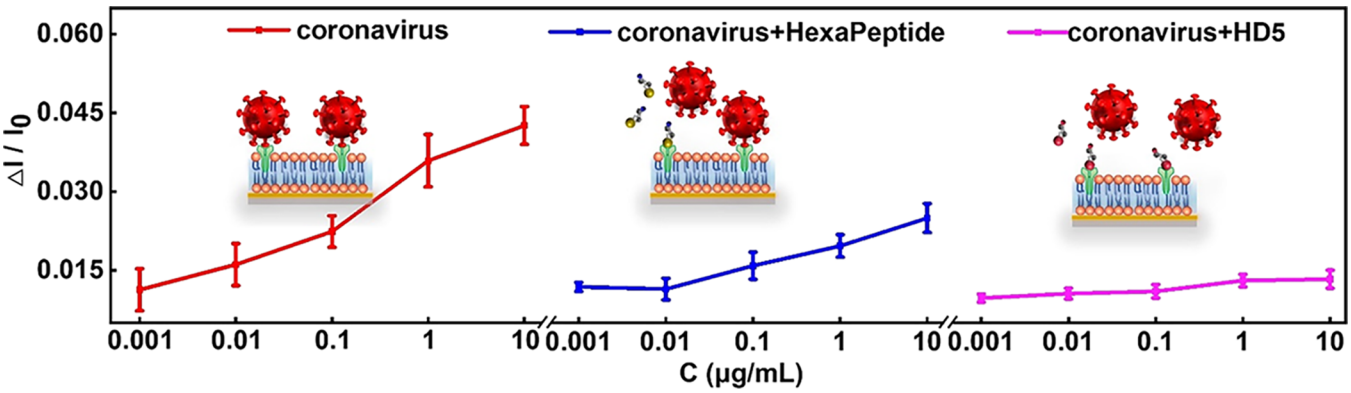

Figure 5. Response of the drug inhibition efficiency of the interaction between coronavirus and ACE2 receptors in the presence of two different drugs. Three inserted illustrations represent different binding of our biosensor, including binding with coronavirus, weak inhibition by the hexapeptide, and strong inhibition by the HD5 peptide.

behavior of biological or nonbiological components such as nanoparticles, proteins, and nucleic acids.

The above results demonstrate that the proposed SLB-based lab-on-a-chip biosensor has the ability of rapid response due to the direct perception of charge change on the lipid membranes, maintains phospholipid membrane activity in vitro, and perfectly simulates cell membrane behavior. All of the above implied that the developed system has great potential to quantify the interaction between the ACE2 receptor and the spike protein and monitor the dynamic behavior of the lipid membrane infected with coronavirus in real time.

Drug Inhibition Test Using the Proposed SLB-Based Lab-on-a-Chip Biosensor. To characterize the performance of our biosensor for the screening of COVID-19 blocking drugs, we further conducted drug inhibition experiments at different concentrations. Previous studies have reported that SARS-CoV-2 directly binds to ACE2 receptors of host cells through spike proteins, facilitating the entry and replication processes. Thus, there are several potential approaches to addressing ACE2 receptor-mediated COVID-19, including TMPRSS2 inhibitors, spike vaccines, soluble ACE2 receptors, and ACE2 receptor blockers.[39] The HD5 peptide and hexapeptide showed high affinity to the host cell surface ACE2 receptors,[40,41] enabling the fourth treatment option possible. Hence, they were employed as inhibition drugs for blocking the interaction between ACE2 receptors and spike proteins of SARS-CoV-2. In this study, the two drugs were used as research objects to verify the evaluation effect of the proposed lab-on-a-chip biosensor for the study of cell inhibition of spike proteins.

As shown in Figure 4a, the real-time current decrease of FET shows that the SLB and ACE2 receptors were embedded on the chip surface, demonstrating the electrical resistance of the SLB and negatively charged ACE2 receptors (Table S1). Then, 1 μg/mL HD5 peptide was added to preempt the ACE2 receptors and the spike proteins at different concentrations were subsequently added. The four plots represent the results of four independent experiments using different HD5 concentrations (0, 0.01, 1, and 10 μg/mL) to evaluate the ability to distinguish the blocking efficiency of the same drug at different concentrations, as shown in Figure 4b. The three HD5 concentrations all showed significant inhibition, and the inhibition efficiency increased with increasing HD5 concentration. Moreover, whether drugs interact with ACE2 receptors or with the spike proteins of SARS-CoV-2 in pharmacology, the system has great potential for the screening of such blocking drugs.

During the drug screening process, the medical half maximal inhibitory concentration (IC_{50}) value was calculated as a quantitative measure that indicates how much of a particular inhibitory substance is needed to inhibit a given biological process or component by up to 50%. To characterize the feasibility of the system for drug IC_{50} quantitative computation, we performed drug IC_{50} tests of HD5 and hexapeptide with gradient concentrations. Following the same procedure mentioned before, after SLB and ACE2 receptors were embedded on the chip surface, the normalized real-time responses of the gradient concentrations (0.0001, 0.001, 0.01, 0.1, 1, and 10 μg/mL) of the two drugs were determined, as shown in Figure 4d,e. Apparently, HD5 responds about three times as well as the hexapeptide at the same concentration, corresponding to the higher affinity, as previously reported. Here, a four-parameter formula (eq 5) model was used to calculate the IC_{50} value of the drug.

$$y = A2 + \frac{A1 - A2}{1 + \left(\frac{x}{x_0}\right)^p} \tag{5}$$

where y is the normalized response and x is the drug concentration. The lower asymptote is $A2$, the bottom of the curve or lower plateau, and the upper asymptote is $A1$, the top of the curve or the upper plateau. The steepness of the linear portion of the curve was described by the slope factor p. The parameter x_0 is the concentration corresponding to the response midway between $A1$ and $A2$.

The statistical average results and the parametric equation fitting between inhibition and drug concentrations are shown in Figure 4c, implying that the IC_{50} value of HD5 (0.2) is significantly smaller than that of hexapeptide (2.2). The IC_{50} value is validated by the QCM-D method (2.98, Figure S8), closely approximating the FET results and reported value (20 nM).[42]

Drug inhibition tests and IC_{50} calculations also indicate the excellent quantitative capability of drug inhibition efficiency.

Screening of Drugs with Viruses. To demonstrate the ability of the virus to respond to a spike protein, we performed the same procedure with transmissible gastroenteritis virus (TGEV). The assembly of SLB, ACE2 receptors, and 1 μg/mL HD5 was performed as previously described. The red plot in Figure 5 shows the response of the introduction of real TGEV

https://doi.org/10.1021/acssensors.2c00970
ACS Sens. XXXX, XXX, XXX−XXX

at different concentrations (ranging from 0.001 to 10 μg/mL), implying a strong interaction between TGEV and the ACE2 receptors of our biosensor.

Furthermore, we performed the same experimental procedure, distinguishing the hexapeptide that was used to replace HD5, to evaluate the capability of our biosensor to screen for better inhibition efficiency of different drugs. The green plot in Figure 5 shows the response of TGEV at different concentrations after the preemptive hexapeptide at a concentration of 1 μg/mL. The hexapeptide-pretreated response was significantly greater than the HD5-pretreated response, illustrating the stronger inhibition efficiency of HD5 due to its higher binding affinity with ACE2 receptors. According to the existing results, it is clear that the proposed lab-on-a-chip biosensor has an excellent performance in detecting real coronavirus samples and calculating the drug inhibition efficiency with different concentrations for the screening of COVID-19 blocking drugs. In general, a variety of similar receptors can be embedded on the SLB to screen for corresponding blocking drugs, which indicates the versatility of our biosensor for other diseases.

CONCLUSIONS

In summary, we have demonstrated a supported lipid bilayer-based lab-on-a-chip biosensor for rapid, label-free electrical detection, which can be used as a platform for the screening of effective inhibition drugs. The construction of SLBs with ACE2 receptors on the surface of the gate electrode serves as a simulated cell environment for biotarget capture and transduction, which perfectly solves the contradiction between the weakening of the binding signal and the interference of nonspecific binding. The stability of detection was dramatically strengthened, which was attributed to the excellent intrinsic properties of the SLB and the uniform orientation of ACE2 receptors. The results indicated that the biosensor exhibits a rapid and sensitive response to the spike protein of coronavirus and presents remarkable capability to quantitatively inhibit spike protein inhibition drugs, even for other similar protein−lipid membrane interaction processes. Therefore, benefiting from the label-free, low-cost, simple, and integrated advantages, the supported lipid bilayer-based lab-on-a-chip biosensor is promising for application in the efficient development of coronavirus drugs in a convenient and easy-to-popularize way.

EXPERIMENTAL SECTION

Reagents and Materials. 1,2-Dioleoyl-*sn*-glycero-3-phosphocholine (DOPC) was purchased from Sigma-Aldrich (USA). The angiotensin-converting enzyme II (ACE2) receptor was purchased from Gene Universal (Anhui, China). Recombinant human novel coronavirus spike glycoprotein (spike protein, molecular weight = 79.6 kDa) with FITC labeled on lysine was purchased from Maiji Biotech (Tianjin, China). Human defensin 5 (HD5) was purchased from Hycult Biotech (Shanghai, China). The hexapeptide was synthesized by Scilight-Peptide (Beijing, China). The simulated coronavirus, transmissible gastroenteritis virus (TGEV), was purchased from Harvac Biotechnology (Harbin, China). All chemicals were used directly without further purification. The DOPC, ACE2 receptors, spike protein, and receptor block peptide all used 1× PBS (phosphate buffer saline, pH = 7.4) as a solvent at 25 °C.

Characterization. The assembly process of the lipid bilayer and ACE2 receptors was monitored using a Q-Sense E1 (Boiling Scientific, Sweden). FRAP experiments were performed by a laser confocal microscope (Leica TCS SP8). SPR experiments were conducted using a P4SPR (Affinity Instruments, Canada). The morphology results were obtained using a NanoWizard 4 (Bruker, Germany) in QI mode using an SLN-10 probe with a 2 nm tip radius and a spring constant of 0.35 N/m.

ASSOCIATED CONTENT

Supporting Information

The Supporting Information is available free of charge at https://pubs.acs.org/doi/10.1021/acssensors.2c00970.

Preparation of vesicles, quartz crystal microbalance (QCM-D) measurements, surface plasmon resonance (SPR) analysis, and atomic force microscopy (AFM) analysis (PDF)

AUTHOR INFORMATION

Corresponding Authors

Xuexin Duan − *State Key Laboratory of Precision Measuring Technology & Instruments, School of Precision Instruments and Optoelectronics Engineering, Tianjin University, Tianjin 300072, China;* orcid.org/0000-0002-7550-3951; Email: xduan@tju.edu.cn

Qiannan Xue − *State Key Laboratory of Precision Measuring Technology & Instruments, School of Precision Instruments and Optoelectronics Engineering, Tianjin University, Tianjin 300072, China;* orcid.org/0000-0001-8688-0018; Email: qiannanxue@tju.edu.cn

Authors

Feng Zhou − *State Key Laboratory of Precision Measuring Technology & Instruments, School of Precision Instruments and Optoelectronics Engineering, Tianjin University, Tianjin 300072, China*

Wenwei Pan − *State Key Laboratory of Precision Measuring Technology & Instruments, School of Precision Instruments and Optoelectronics Engineering, Tianjin University, Tianjin 300072, China*

Ye Chang − *State Key Laboratory of Precision Measuring Technology & Instruments, School of Precision Instruments and Optoelectronics Engineering, Tianjin University, Tianjin 300072, China*

Xueyou Su − *State Key Laboratory of Precision Measuring Technology & Instruments, School of Precision Instruments and Optoelectronics Engineering, Tianjin University, Tianjin 300072, China*

Complete contact information is available at: https://pubs.acs.org/10.1021/acssensors.2c00970

Notes

The authors declare no competing financial interest.

ACKNOWLEDGMENTS

The authors gratefully acknowledge financial support from the National Key R&D Program of China (2021YFC3002202), the 111 Project (B07014), and The Scientific Research Transformation Foundation of Wenzhou Safety (Emergency) Institute of Tianjin University.

REFERENCES

(1) Shang, J.; Ye, G.; Shi, K.; Wan, Y.; Luo, C.; Aihara, H.; Geng, Q.; Auerbach, A.; Li, F. Structural basis of receptor recognition by SARS-CoV-2. *Nature* **2020**, *581*, 221−224.

(2) Hamming, I.; Timens, W.; Bulthuis, M. L. C.; Lely, A. T.; Navis, G. J.; van Goor, H. Tissue distribution of ACE2 protein, the

functional receptor for SARS coronavirus. A first step in understanding SARS pathogenesis. *J. Pathol.* **2004**, *203*, 631−637.
(3) Walls, A. C.; Park, Y. J.; Tortorici, M. A.; Wall, A.; McGuire, A. T.; Veesler, D. Structure, Function, and Antigenicity of the SARS-CoV-2 Spike Glycoprotein. *Cell* **2020**, *181*, 281−292.e6.
(4) Renaud, J. P.; Chari, A.; Ciferri, C.; Liu, W. T.; Rémigy, H. W.; Stark, H.; Wiesmann, C. Cryo-EM in drug discovery: Achievements, limitations and prospects. *Nat. Rev. Drug Discovery* **2018**, *17*, 471−492.
(5) Pereira, S. A. P.; Dyson, P. J.; Saraiva, M. L. M. F. S. Miniaturized technologies for high-throughput drug screening enzymatic assays and diagnostics − A review. *TrAC, Trends Anal. Chem.* **2020**, *126*, No. 115862.
(6) Chen, L.; Lv, D.; Wang, S.; Wang, D.; Chen, X.; Liu, Y.; Hong, Z.; Zhu, Z.; Cao, Y.; Chai, Y. Surface Plasmon Resonance-Based Membrane Protein-Targeted Active Ingredients Recognition Strategy: Construction and Implementation in Ligand Screening from Herbal Medicines. *Anal. Chem.* **2020**, *92*, 3972.
(7) Chen, C.; Lagae, L.; Maes, G.; Borghs, G.; Van Dorpe, P. Highly confined surface plasmon polariton resonances in rectangular nanopore cavities. *Phys. Status Solidi RRL* **2010**, *4*, 247−249.
(8) Verzijl, D.; Riedl, T.; Parren, P. W. H. I.; Gerritsen, A. F. A novel label-free cell-based assay technology using biolayer interferometry. *Biosens. Bioelectron.* **2017**, *87*, 388−395.
(9) Zhang, C.; Xu, J. Q.; Li, Y. T.; Huang, L.; Pang, D. W.; Ning, Y.; Huang, W. H.; Zhang, Z.; Zhang, G. J. Photocatalysis-Induced Renewable Field-Effect Transistor for Protein Detection. *Anal. Chem.* **2016**, *88*, 4048−4054.
(10) Kuo, C. J.; Chiang, H. C.; Tseng, C. A.; Chang, C. F.; Ulaganathan, R. K.; Ling, T. T.; Chang, Y. J.; Chen, C. C.; Chen, Y. R.; Chen, Y. T. Lipid-Modified Graphene-Transistor Biosensor for Monitoring Amyloid-β Aggregation. *ACS Appl. Mater. Interfaces* **2018**, *10*, 12311−12316.
(11) Zong, X.; Zhu, R. ZnO nanorod-based FET biosensor for continuous glucose monitoring. *Sens. Actuators, B* **2018**, *255*, 2448−2453.
(12) Bhattacharyya, I. M.; Cohen, S.; Shalabny, A.; Bashouti, M.; Akabayov, B.; Shalev, G. Specific and label-free immunosensing of protein-protein interactions with silicon-based immunoFETs. *Biosens. Bioelectron.* **2019**, *132*, 143−161.
(13) Chen, C. P.; Ganguly, A.; Lu, C. Y.; Chen, T. Y.; Kuo, C. C.; Chen, R. S.; Tu, W. H.; Fischer, W. B.; Chen, K. H.; Chen, L. C. Ultrasensitive in situ label-free DNA detection using a GaN nanowire-based extended-gate field-effect-transistor sensor. *Anal. Chem.* **2011**, *83*, 1938−1943.
(14) Chiu, Y. S.; Tseng, C. Y.; Lee, C. T. Nanostructured EGFET pH sensors with surface-passivated ZnO thin-film and nanorod array. *IEEE Sens. J.* **2012**, *12*, 930−934.
(15) Sharma, P.; Gupta, S.; Singh, R.; Ray, K.; Kothari, S. L.; Sinha, S.; Sharma, R.; Mukhiya, R.; Awasthi, K.; Kumar, M. Hydrogen ion sensing characteristics of Na3BiO4−Bi2O3 mixed oxide nanostructures based EGFET pH sensor. *Int. J. Hydrogen Energy* **2020**, *45*, 18743−18751.
(16) Zhang, Q.; Liu, W.; Sun, C.; Zhang, H.; Pang, W.; Zhang, D.; Duan, X. On-chip surface modified nanostructured ZnO as functional pH sensors. *Nanotechnology* **2015**, *26*, No. 355202.
(17) Tarasov, A.; Tsai, M. Y.; Flynn, E. M.; Joiner, C. A.; Taylor, R. C.; Vogel, E. M. Gold-coated graphene field-effect transistors for quantitative analysis of protein-antibody interactions. *2D Mater.* **2015**, *2*, No. 044008.
(18) Minamiki, T.; Ichikawa, Y.; Kurita, R. Systematic Investigation of Molecular Recognition Ability in FET-Based Chemical Sensors Functionalized with a Mixed Self-Assembled Monolayer System. *ACS Appl. Mater. Interfaces* **2020**, *12*, 15903−15910.
(19) Capua, L.; Locca, D.; Ionescu, A. Antibodies fragments as enablers of cardiac troponin (cTn) detection with extended gate metal-oxide-semiconductor field effect transistors (EGFET). *Eur. Heart J.* **2020**, *41*, ehaa946-1699.
(20) Tamboli, V. K.; Bhalla, N.; Jolly, P.; Bowen, C. R.; Taylor, J. T.; Bowen, J. L.; Allender, C. J.; Estrela, P. Hybrid synthetic receptors on MOSFET devices for detection of prostate specific antigen in human plasma. *Anal. Chem.* **2016**, *88*, 11486−11490.
(21) Wang, Y. Y.; Pham, T. D.; Zand, K.; Li, J.; Burke, P. J. Charging the quantum capacitance of graphene with a single biological ion channel. *ACS Nano* **2014**, *8*, 4228−4238.
(22) Korman, C. E.; Megens, M.; Ajo-Franklin, C. M.; Horsley, D. A. Nanopore-spanning lipid bilayers on silicon nitride membranes that seal and selectively transport ions. *Langmuir* **2013**, *29*, 4421−4425.
(23) Huang, Y.; Palkar, P. V.; Li, L. J.; Zhang, H.; Chen, P. Integrating carbon nanotubes and lipid bilayer for biosensing. *Biosens. Bioelectron.* **2010**, *25*, 1834−1837.
(24) Bally, M.; Graule, M.; Parra, F.; Larson, G.; Höök, F. A virus biosensor with single virus-particle sensitivity based on fluorescent vesicle labels and equilibrium fluctuation analysis. *Biointerphases* **2013**, *8*, 4.
(25) Khorshid, M.; Losada-Pérez, P.; Wackers, G.; Yongabi, D.; Renner, F. U.; Thoelen, R.; Wagner, P. Real-time monitoring of interactions between Ebola fusion peptide and solid-supported phospholipid membranes: Effect of peptide concentration and layer geometry. *Phys. Med.* **2017**, *4*, 1−7.
(26) Heider, S.; Reimhult, E.; Metzner, C. Real-time analysis of protein and protein mixture interaction with lipid bilayers. *Biochim. Biophys. Acta, Biomembr.* **2018**, *1860*, 319−328.
(27) Yu, X.; Xia, Y.; Tang, Y.; Zhang, W.-L.; Yeh, Y.-T.; Lu, H.; Zheng, S.-Y. A Nanostructured Microfluidic Immunoassay Platform for Highly Sensitive Infectious Pathogen Detection. 2017, *12*, 1700425, DOI: 10.1002/smll.201700425.
(28) Hartley, M. D.; Schneggenburger, P. E.; Imperiali, B. Lipid bilayer nanodisc platform for investigating polyprenol-dependent enzyme interactions and activities. *Proc. Natl. Acad. Sci. U. S. A.* **2013**, *110*, 20863−20870.
(29) Zhang, J.; Wang, X.; Chen, T.; Feng, C.; Li, G. Electrochemical Analysis of Enzyme Based on the Self-Assembly of Lipid Bilayer on an Electrode Surface Mediated by Hydrazone Chemistry. *Anal. Chem.* **2017**, *89*, 13245−13251.
(30) Wu, J. C.; Tseng, P. Y.; Tsai, W. S.; Liao, M. Y.; Lu, S. H.; Frank, C. W.; Chen, J. S.; Wu, H. C.; Chang, Y. C. Antibody conjugated supported lipid bilayer for capturing and purification of viable tumor cells in blood for subsequent cell culture. *Biomaterials* **2013**, *34*, 5191−5199.
(31) Yeh, P. Y.; Chen, Y. R.; Wang, C. F.; Chang, Y. C. Promoting Multivalent Antibody-Antigen Interactions by Tethering Antibody Molecules on a PEGylated Dendrimer-Supported Lipid Bilayer. *Biomacromolecules* **2018**, *19*, 426−437.
(32) Di Iorio, D.; Verheijden, M. L.; Van Der Vries, E.; Jonkheijm, P.; Huskens, J. Weak Multivalent Binding of Influenza Hemagglutinin Nanoparticles at a Sialoglycan-Functionalized Supported Lipid Bilayer. *ACS Nano* **2019**, *13*, 3413−3423.
(33) Toyoda, Y.; Morimoto, K.; Suno, R.; Horita, S.; Yamashita, K.; Hirata, K.; Sekiguchi, Y.; Yasuda, S.; Shiroishi, M.; Shimizu, T.; Urushibata, Y.; Kajiwara, Y.; Inazumi, T.; Hotta, Y.; Asada, H.; Nakane, T.; Shiimura, Y.; Nakagita, T.; Tsuge, K.; Yoshida, S.; Kuribara, T.; Hosoya, T.; Sugimoto, Y.; Nomura, N.; Sato, M.; Hirokawa, T.; Kinoshita, M.; Murata, T.; Takayama, K.; Yamamoto, M.; Narumiya, S.; Iwata, S.; Kobayashi, T. Ligand binding to human prostaglandin E receptor EP 4 at the lipid-bilayer interface. *Nat. Chem. Biol.* **2019**, *15*, 18−26.
(34) Kaisti, M. Detection principles of biological and chemical FET sensors. *Biosens. Bioelectron.* **2017**, *98*, 437−448.
(35) Hanaor, D. A. H.; Ghadiri, M.; Chrzanowski, W.; Gan, Y. Scalable surface area characterization by electrokinetic analysis of complex anion adsorption. *Langmuir* **2014**, *30*, 15143−15152.
(36) Hu, S. K.; Lo, F. Y.; Hsieh, C. C.; Chao, L. Sensing Ability and Formation Criterion of Fluid Supported Lipid Bilayer Coated Graphene Field-Effect Transistors. *ACS Sens.* **2019**, *4*, 892−899.
(37) Ang, P. K.; Jaiswal, M.; Lim, C. H. Y. X.; Wang, Y.; Sankaran, J.; Li, A.; Lim, C. T.; Wohland, T.; Barbaros, Ö.; Loh, K. P. A

https://doi.org/10.1021/acssensors.2c00970
ACS Sens. XXXX, XXX, XXX−XXX

bioelectronic platform using a graphene-lipid bilayer interface. *ACS Nano* **2010**, *4*, 7387−7394.
(38) Jang, H.; Lee, T.; Song, J.; Russell, L.; Li, H.; Dailey, J.; Searson, P. C.; Katz, H. E. Electronic Cortisol Detection Using an Antibody-Embedded Polymer Coupled to a Field-E ff ect Transistor. 2018, 16233−16237, DOI: 10.1021/acsami.7b18855.
(39) Zhang, H.; Penninger, J. M.; Li, Y.; Zhong, N.; Slutsky, A. S. Angiotensin-converting enzyme 2 (ACE2) as a SARS-CoV-2 receptor: molecular mechanisms and potential therapeutic target. *Intensive Care Med.* **2020**, *46*, 586−590.
(40) Wang, C.; Wang, S.; Li, D.; Zhao, X.; Han, S.; Wang, T.; Zhao, G.; Chen, Y.; Chen, F.; Zhao, J.; Wang, L.; Sun, W.; Huang, Y.; Su, Y.; Wei, D.; Zhao, J.; Wang, J. Lectin-like Intestinal Defensin Inhibits 2019-nCoV Spike binding to ACE2. 2020, bioRxiv. https://www.biorxiv.org/content/10.1101/2020.03.29.013490v1.
(41) Struck, A. W.; Axmann, M.; Pfefferle, S.; Drosten, C.; Meyer, B. A hexapeptide of the receptor-binding domain of SARS corona virus spike protein blocks viral entry into host cells via the human receptor ACE2. *Antiviral Res.* **2012**, *94*, 288−296.
(42) Rajabi, M.; Ericksen, B.; Wu, X.; De Leeuw, E.; Zhao, L.; Pazgier, M.; Lu, W. Functional determinants of human enteric α-defensin HD5: Crucial role for hydrophobicity at dimer interface. *J. Biol. Chem.* **2012**, *287*, 21615−21627.

https://doi.org/10.1021/acssensors.2c00970
ACS Sens. XXXX, XXX, XXX−XXX